Advances in Science and Technology Research Journal

Advances in Science and Technology Research Journal 2022, 16(5), 163–177
https://doi.org/10.12913/22998624/154025
ISSN 2299-8624, License CC-BY 4.0

Received: 2022.07.19
Accepted: 2022.10.17
Published: 2022.11.01

An Elastic-Plastic Analysis of Polycrystalline Structure Using Crystal Plasticity Modelling – Theory and Benchmark Tests

Marta Wójcik[1*], Andrzej Skrzat[1]

[1] Department of Materials Forming and Processing, Rzeszow University of Technology, al. Powstańców Warszawy 8, 35-959 Rzeszów, Poland

* Corresponding author's e-mail: m.wojcik@prz.edu.pl

ABSTRACT

Numerical simulations of tension and shear tests for a polycrystalline, anisotropic material were performed using crystal plasticity theory. The slip was considered here as the main mechanism of plastic deformation. Constitutive equations to describe the elastic-plastic deformation caused by the slip are presented. The generation and meshing of various shapes geometries (cubic and paddy shapes) with randomly-orientated grains by means of open source software NEPER program was shown. The Voronoi tessellation was used in order to include morphological properties of a crystalline material. The selected results of elastic-plastic analyses (stress, strain distributions and the macroscopic stress-strain resulting from homogenization) are presented here. The results obtained show the non-uniform distribution of stress and strain for different grains associated with their crystal orientation. The crystal plasticity finite element modelling of materials subjected to plastic deformation is important for microstructure-based mechanical predictions, as well as for the engineering design and to perform simulations involving not only the change of a material's shape at a macro level but also the phenomena occurring in material in a micro-scale.

Keywords: crystal plasticity, polycrystalline material, slip system modelling, plastic deformation, microstructure, anisotropy.

INTRODUCTION

In numerical analyses of elastic-plastic problems including metal forming processes, classical plasticity theory or unified plasticity one might be applied. The first ones enable to describe the behaviour of materials under loading in macro scale only without considering the micro-mechanism occurring in a material during deformation which is the goal of unified plasticity approaches. The change of a material microstructure gives the full explanation of plastic deformation process [1–2]. In turns, unified plasticity models assume not only the change of the material shape under loading in a macro scale, but also the change of its microstructure, strain hardening and anisotropy caused by the plastic deformation mechanisms, e.g. slip and twinning [3]. These models describe the elastic-plastic behaviour of materials linking different scales of the problem – from macro- to micro- or even to nano- levels (Figure 1).

The important issue in modelling of material polycrystalline microstructure is the description of the interaction between particular grains. A variety of micromechanical models have been proposed so far. In Taylor model [4], the strain is the same in all grains and equals to the global strain. It is assumed that every grain deforms in the same way as the representative volume element. However, the equilibrium equations on grain boundaries are not satisfied in this approach. The Sachs model [5] assumes that the stress state for all grains is the same and equals the global stress state of the material which causes the discontinuity of a displacement. In another model based on the self-consistent approach [6], every grain is considered as an ellipsoidal heterogeneity which is placed in a uniform space representing the polycrystalline

structure. The multiplicative decomposition of the total deformation gradient into elastic and plastic parts assuming also twinning is described by Khan et al. [7]. Other more advance micromechanical models assume that some components of stress or strain states are the same or use the homogenization theory for the determination of stress and strain distributions in crystals [8–9]. For example, a micromorphic model of crystal plasticity by combining the microcurl model with the minimal gradient-enhancement of the hardening law has been proposed by Ryś et al. [10]. In this approach, the condition for the plastic flow was introduced using the assumed compatibility of actual and virtual dissipation rates. The crystal plasticity model with one yield surface expressed by the homogeneous yield function of degree 2n was described by Kowalczyk-Gajewska et al. [11]. The constitutive model formulated within the large-strain crystal plasticity framework is presented by Kowalczyk-Gajewska et al. [12]. More information about crystal plasticity models is contained in papers [13–15].

Metals considered in this paper are polycrystalline materials in which the elementary volume element consists of a large amount of grains with a crystalline structure [16]. The single crystal constitutes a three-dimensional arrangement of atoms – FCC (face centered cubic), BCC (body centered cubic) or HCP (hexagonal close packed) [17]. Mechanical properties of metals, especially the ability to plastic deformation, depend on their crystalline structure. The crystal plasticity (CP) theory gives the explanation of many mechanical phenomena on the continuum body level and enables to estimate quantitative evaluation of mechanical properties [18].The dislocation slip (considered in this paper) and the twinning (not included here) are the main mechanisms of the plastic deformation in metals. Anisotropic slip occurs only on selected crystalline planes and in selected directions within these planes (slip systems). The slip systems are preferred in directions most densely packed by atoms. Depending on the crystalline structure, polycrystals have different number of slip systems defined by *n* and *m* normalized vectors. The *n* vector is normal to the slip plane and *m* vector is parallel to the slip direction [19]. The slip systems are related with the crystalline network of a metal [20]. The number of slip planes, directions and slip systems for three main crystalline structures are summarized in Table 1. The FCC structure considered in this paper is defined by four slip planes and for three slip directions on these planes, which gives twelve- slip systems (Figure 2) [21]. The plastic deformation occurs more easily in crystals with higher number of the slip systems, especially when they are located more favorably against the direction of a load.

The slip does not change the orientation of a crystalline structure and all atoms in a lattice maintain the same distance with each other (Figure 3).

The plastic deformation caused by the dislocation slip is a result of a shear posed by the shearing stress – resolved shear stress (τ_{RSS}). According to the Schmidt law, the slip occurs when shear stresses on selected slip plane and in selected slip direction reach the critical value – the critical resolved shear stress (τ_{CRSS}) [22]. The condition which determines the occurrence of a slip in selected slip system is as follows (Eq. 1) [23]:

$$\tau_{RSS} > \tau_{CRSS} \tag{1}$$

where:

$$\tau_{RSS} = \sigma cos\varphi cos\lambda \tag{2}$$

where: σ – a tensile stress,
λ – an angle between tensile axis and the slip direction (Figure 4),

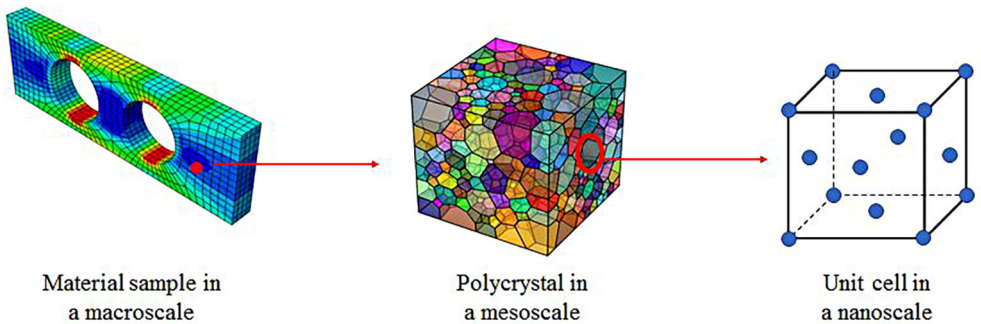

Fig. 1. The idea of a multi-scale crystal plasticity

Table 1. Crystalline structures and their number of slip planes, directions and systems

Crystalline structure	Number of slip planes	Number of slip directions	Number of slip systems
FCC (face centered cubic) – A1	4	3	12
BCC (body centered cubic) – A2	6	2	12
	12	1	12
	24	1	24
HCP (hexagonal close packed) – A3	1	3	3
	3	1	3
	6	1	6

ϕ – an angle between tensile angle and the slip plane normal. The part $cos\varphi cos\lambda$ in Eq. 2 defines the Schmidt factor (S^{α}). It is worth highlighting that the dislocation slip is not activated in all slip systems simultaneously. The slip starts in the system for which the Schmidt factor has the highest value. Another slip systems might be initiated later on under further loading.

The deformation caused by the dislocation motion also leads to the rotation of a material together with the shearing [24].

The aim of this research work is a numerical elastic-plastic analysis of polycrystalline anisotropic material –C11000 copper alloy of FCC (A1) crystalline structure commonly used in many industrial applications and characterized by the minimum Cu weight concentration of 99%. The morphology was defined by means of the Voronoi tessellation. The random distribution of grains orientation was assumed. The numerical calculations of an uniaxial loading and a shear test including elastic and plastic parameters for a copper was performed by the FEPX software. The constitutive equations of a single crystal plasticity theory assume dislocation slip as the only mechanism of a plastic deformation. The

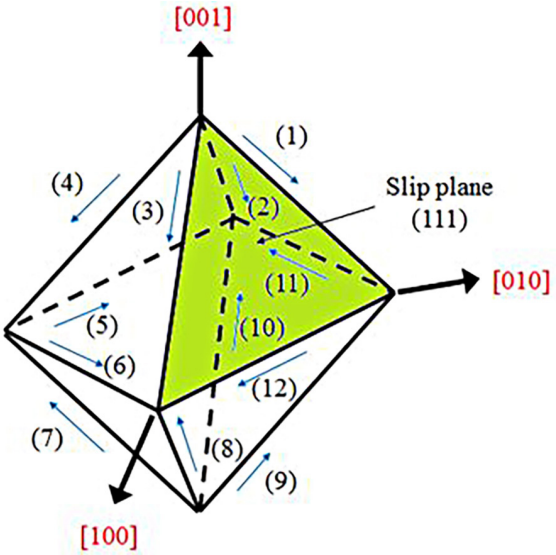

Fig. 2. Slip planes and slip directions for FCC structure considered in this paper

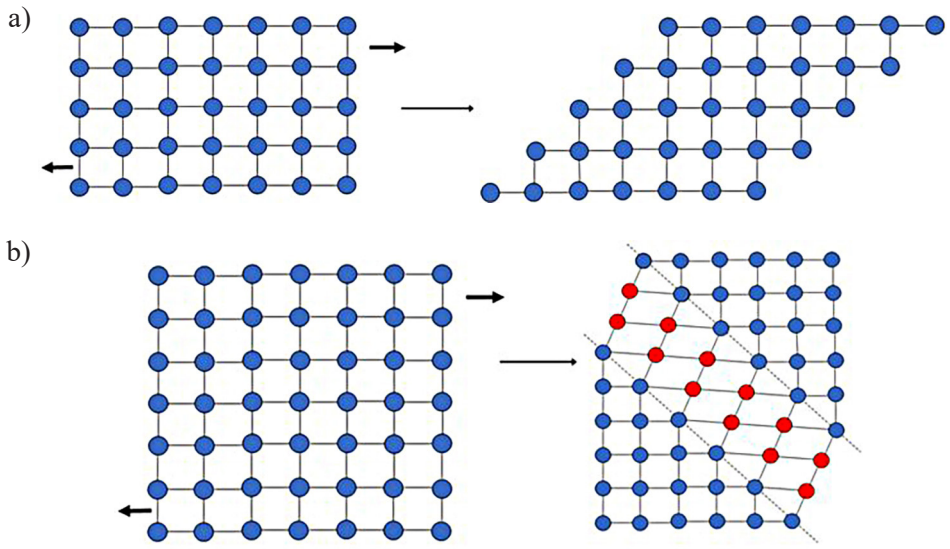

Fig. 3. The comparison of the lattice crystal orientation during a slip (a) and a twinning (b)

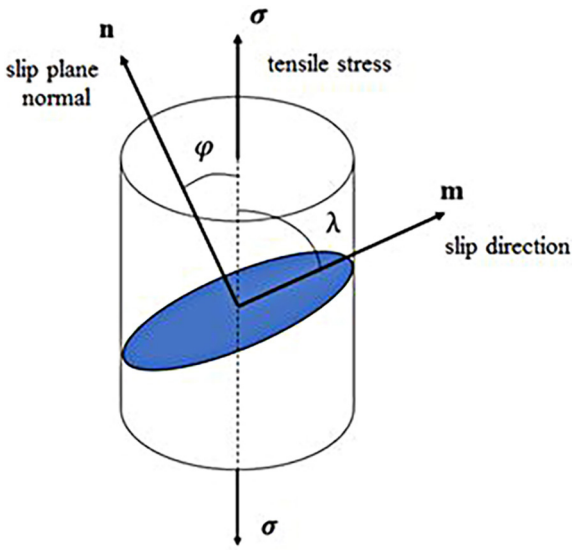

Fig. 4. Definition of the resolved shear stress

modelling assuming both slip and twinning are described in papers [25–27]. The benchmark tests were performed for different model shapes –cubic and paddy shapes. The results obtained show the potential of crystal plasticity modelling as a numerical tool to solve a wide range of engineering problems, e.g modeling of materials forming processes, severe plastic deformation (SPD) analyses, super plasticity problems etc. considering phenomena occurring in materials in macro- and nano- scales. Such an analysis provides a more complete description of the material behavior than classical macromechanical plasticity theory at a small scale.

CONSTITUTIVE EQUATIONS OF A CRYSTAL PLASTICITY THEORY

The viscoplastic crystalline plastic model considering 12 slip systems for a single crystal with FCC structure is applied here. The constitutive equations based on the CP theory are as follows:

1. The multiplicative decomposition of the deformation gradient F into its elastic F^e and plastic components F^p (Eq. 3):

$$F = F^e F^p \tag{3}$$

The elastic deformation gradient includes the elastic stretching and rigid body rotation [28]. The plastic part F^p which occurs after removing the load, describes the plastic shear of the material (see Figure 5 fora uniaxial example) [29]. The plastic deformation gradient also contains information about the dislocations arising in the slip systems [30].

2. The macroscopic velocity gradient for a material point of a crystal grain can be additively decomposed into the elastic and plastic components, L^e and L^p, respectively, as follows (Eq. 4–6):

$$L = L^e + L^p \tag{4}$$

where:

$$L^e = \dot{F}^e (F^e)^{-1} \tag{5}$$

$$L^p = F^e \dot{F}^p (F^p)^{-1} (F^e)^{-1} \tag{6}$$

where: the dot means time derivative.

3. The Euler's velocity gradient tensor L might be decomposed into a symmetric deformation velocity tensor D and the antisymmetric spin tensor Ω (Eq. 7–9):

$$L = D + \Omega \tag{7}$$

where:

$$D = sym(L) = \frac{1}{2}(L + L^T) \tag{8}$$

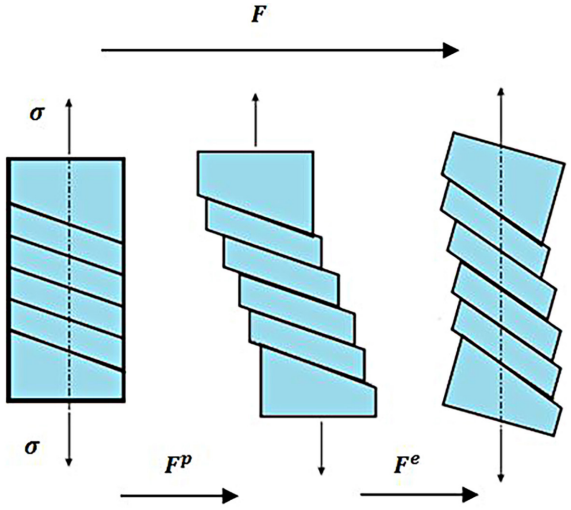

Fig. 5. Elastic-plastic deformation of a single crystal during an uniaxial test

$$\Omega = asym(L) = \frac{1}{2}(L - L^T) \tag{9}$$

Subsequently, deformation velocity gradient and spin tensors can be decomposed into a lattice contribution elastic part and plastic one (Eq. 10–11).

$$D = D^e + D^p \tag{10}$$

$$\Omega = \Omega^e + \Omega^p \tag{11}$$

The plastic spin tensor Ω^p is derived from the crystal slip and the elastic spin one Ω^e can be defined in line with Eq. 12:

$$\Omega^e = R \cdot \dot{R}^T \tag{12}$$

where: R – a rigid body rotation of a crystalline lattice,
Ω^e – describes the evolution of the orientation of the crystallographic lattice [31].

4. It is assumed that the plastic deformation caused by the dislocation slip changes neither the geometry nor the orientation of a crystal and the lattice undergoes the only elastic deformation [32]. Using the polar decomposition, the elastic part of a deformation gradient can be written as a multiplication of a rigid body tensor R^e and the right stretching tensor U^e (Eq. 13).

$$F^e = R^e U^e \tag{13}$$

As mentioned before, the crystal plasticity connects problems of different scales. The plastic velocity gradient is calculated as a sum of slip rates on all slip systems and this way links the macro- and micro- scales (Eq. 14) [25, 33].

$$L^p = \sum_{\alpha=1}^{n} \dot{\gamma}^\alpha m^\alpha \otimes n^\alpha = \sum_{\alpha=1}^{n} \dot{\gamma}^\alpha S^\alpha \tag{14}$$

where: $\dot{\gamma}^\alpha$ – denotes the shearing rate on the α slip system,
m^α – a slip direction,
n^α – a slip plane normal,
S^α – the Schmidt tensor for the α slip system,
n – a total number of slip systems. It is assumed that m^α and n^α are orthogonal (Eq. 15):

$$m^\alpha \cdot n^\alpha = 0 \tag{15}$$

Assuming the connection between macro- and micro- scales, the plastic deformation velocity gradient D^p and the plastic spin Ω^p tensors can be expressed as follows (Eq. 16–17) [34]:

$$D^p = \frac{1}{2}(L^p + L^{pT}) = \sum_{\alpha=1}^{n} p^\alpha \cdot \dot{\gamma}^\alpha \tag{16}$$

$$\Omega^p = \frac{1}{2}(L^p - L^{pT}) = \sum_{\alpha=1}^{n} \omega^\alpha \cdot \dot{\gamma}^\alpha \tag{17}$$

where: p^α and ω^α – symmetric and asymmetric tensors defining the Schmidt tensor on a selected α slip system.

Similarly, the elastic deformation velocity gradient associated with the stretching and the elastic (lattice) spin can be defined by the following (Eq. 18–19) [34]:

$$D^e = \frac{1}{2}(L^e + L^{eT}) = D - \sum_{\alpha=1}^{n} p^\alpha \cdot \dot{\gamma}^\alpha \tag{18}$$

$$\Omega^e = \frac{1}{2}(L^e - L^{eT}) = \Omega - \sum_{\alpha=1}^{n} \omega^\alpha \cdot \dot{\gamma}^\alpha \tag{19}$$

The numerical calculations of elastic-plastic problems based on the CP theory using equations above (Eq. 3–19) are time-consuming and complex, and require a lot of computation steps. The complexity of crystal plasticity FEM (CPFEM) approaches is shown in Figure 6. The calculations are made iteratively in a loop. Depending on the method applied (explicit or implicit), the aim of increment is the calculation of stress required to reach the final deformation gradient and/or the determination of the Jacobian matrix $J = \frac{\partial \Delta\sigma}{\partial \Delta\varepsilon}$ (the implicit method only) [35].

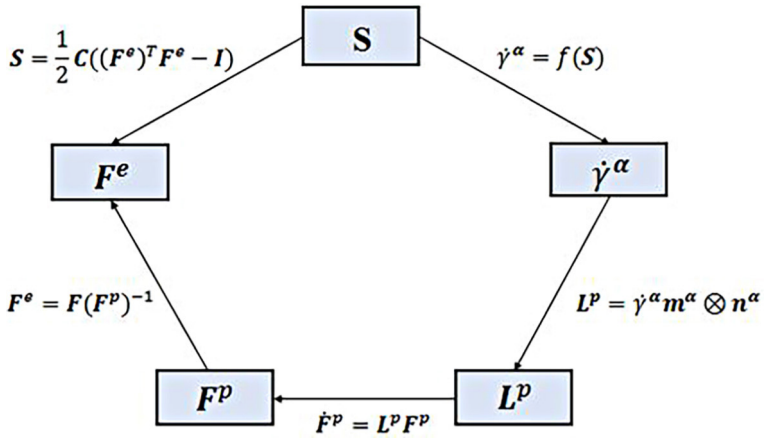

Fig. 6. Diagram showing calculations during the stress determination using the crystal plasticity theory

One can see in Figure 6 that the plastic velocity deformation gradient expressed by a shear rate in the slip systems is required to update the stress tensor. On the other hand, the second Piola-Kirchoff stress tensor S is calculated from L_p, F_p and F_e tensors (Eq. 20):

$$S = CE^e = \frac{1}{2}C((F^e)^T F^e - I) \tag{20}$$

where: C – the elasticity tensor,
E^e – the symmetric elastic strain tensor,
I – the identity matrix.

The yield condition for a single crystal is defined by the classical Schmidt law or by the regulated Schmidt one [36–37]. According to the first one, a single crystal yields when the resolved shear stress τ_{RSS} reaches the τ_{CRSS} critical value and is defined as follows (Eq. 21):

$$\max(\tau_{RSS}) = \tau_{CRSS} \text{ and } \dot{\tau}_{RSS} = 0 \tag{21}$$

In line with the regulated Schmidt law, the yield condition is expressed in the following (Eq. 22):

$$f(\sigma) - m = \sum \left(\frac{\tau_{RSS}}{\tau_{CRSS}}\right)^{2n} - m = 0 \quad \text{and } f(\sigma) = m, \dot{f} = 0 \tag{22}$$

where: m and n – material constants.

Strain hardening of a material is the result of an increase in the slip resistance. According to Dawson et al. [38], the shear rate for a slip system evaluates as follows (Eq. 23):

$$\dot{\gamma}^\alpha = \dot{\gamma}_0 \left(\frac{|\tau^\alpha|}{g^\alpha}\right)^k sgn(\tau^\alpha) \tag{23}$$

where: $\dot{\gamma}_0$ – a reference shear strain rate on the α slip system,
τ^α – a resolved shear stress on the α slip system,
k – the rate sensitivity coefficient,
g^α – the critical shear stress on the α activated slip system to govern the isotropic hardening of the crystal.

The shear rate, including also the effect of a backstress associated with the kinematic hardening, is written by the following (Eq. 24):

$$\dot{\gamma}^\alpha = \dot{\gamma}_0 sgn(\tau^\alpha - x^\alpha) \left(\frac{|\tau^\alpha - x^\alpha|}{g^\alpha}\right)^k \tag{24}$$

where: x^α – a backstress which characterizes the nonlinear kinematic (directional) hardening of the crystal on the α slip system. Its evolution defined by Walker and Chaboche is expressed as (Eq. 25) [39]:

$$x = a\dot{\gamma}^\alpha - c[1 - e_1(1 - \exp(-e_2\gamma))]x^\alpha|\dot{\gamma}^\alpha| - dx^\alpha \tag{25}$$

where: a – the initial hardening modulus of a slip system,
c – the nonlinear hardening parameter,
c_1 and c_2 – describe the cyclic hardening saturation.

The evolution of a slip system strength (g^α) for a given activated slip is the following (Eq. 26) [40]:

$$\dot{g}^{\alpha} = h_0 \left(\frac{g_s(\dot{\gamma}) - g^{\alpha}}{g_s(\dot{\gamma}) - g_0} \right)^{n} g_0 \tag{26}$$

where: h_0 – the fixed-state hardening rate scaling coefficient, g_0 – the initial slip system strength and n is a non-linear Voce hardening exponent.

The slip system saturation strength $g_s(\dot{\gamma})$ is as follows (Eq. 27) [41]:

$$g_s(\dot{\gamma}) = g_{s0} \left(\frac{\dot{\gamma}}{\dot{\gamma}_{s0}} \right)^{m'} \tag{27}$$

where: g_{s0} – the initial slip system saturation strength,
m' – a saturation strength rate scaling exponent,
$\dot{\gamma}_{s0}$ – the initial saturation slip system shear rate,
$\dot{\gamma}$ – a sum of $\dot{\gamma}^{\alpha}$ values.

The constitutive equations presented above are implemented in open source FEPX software used here in numerical computations of selected elastic-plastic problems.

NUMERICAL MODELLING OF CRYSTAL PLASTICITY

Numerical simulations presented in this paper were carried out for the C11000 copper alloy modelled as a polycrystalline material with the FCC structure. Its elastic and plastic parameters taken from literature are contained in Table 2.

The crystal plasticity finite element simulations were carried out using NEPER as a pre- and post- processor, and FEPX as a solver. In NEPER program, the geometry is modelled by polycrystals obtained by means of 3D Voronoi tessellation. Finite element mesh generated by NEPER, as well as the analysis data and boundary conditions are applied as input files to FEPX program. This finite element solver allows modelling macro- and nano-mechanical behaviours of large polycrystalline aggregates with complex microstructures assuming their crystallographic characteristics, e.g. slip systems, hardening and anisotropy of grains. The FEPX acts as a simulation tool for a NEPER. The stages of elastic-plastic analyses used in this paper are presented in Figure 7.

The crystal plasticity (CP) constitutive phenomenological model with elastic part based on the generalized Hook's law and plastic part assuming flow and hardening rules, as well as the yield condition (see equations above) was used here.

Numerical simulations were done for a cubic and a paddy-like geometrical models. Different numbers of grains (400 and 800 grains) with the random morphology, size and random crystal orientations were applied here. For geometries mentioned above, an uniaxial loading test and shear test were done.

BENCHMARK TESTS

In the first benchmark test, the cubic representative volume element (RVE) of dimensions 1 × 1 × 1 mm was used. Two cases were investigated where the RVE was divided into 400 and 800 grains as shown in Figure 8. The grain size was differential in the range of 30–150 μm. Each grain is a monocrystalline, i.e. all finite elements inside a grain have the same crystal orientations. The finite element meshes consisting of tetrahedral elements are shown in Figure 9. Details of FEM models are included in Table 3.

In the tension test the following boundary conditions corresponding to the specimen mounting in the testing machine are applied:

$u_x = u_y = u_z = 0$ on the bottom face (z = 0),

$u_x = u_y = 0$, $u_z = 0.02$ mm (corresponds to the axial strain of 2%) on the upper face (z = 1).

The σ_{zz} stress acting on the loading direction for 400 and 800 grain models is shown in Figure 10. One can see that the distribution of stress is not regular. On the bottom and upper faces the influence of applied boundary conditions

Table 2. Elastic and plastic parameters for a C11000 copper alloy used in this research

Elastic parameters	
E [MPa]	$1.66 \cdot 10^5$
v [-]	0.33
Plastic parameters	
m [-]	0.05
$\dot{\gamma}_0$ [1/s]	1
h_0 [MPa]	200
g_0 [MPa]	210
g_{s0} [MPa]	330
n [-]	1

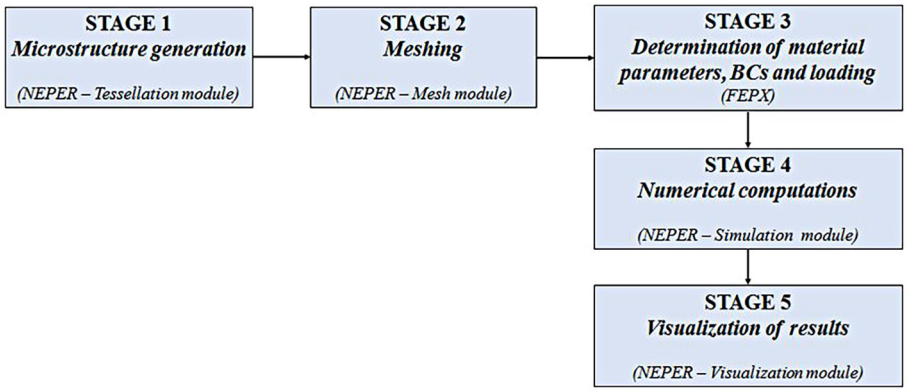

Fig. 7. The stages of numerical analyses used in this paper

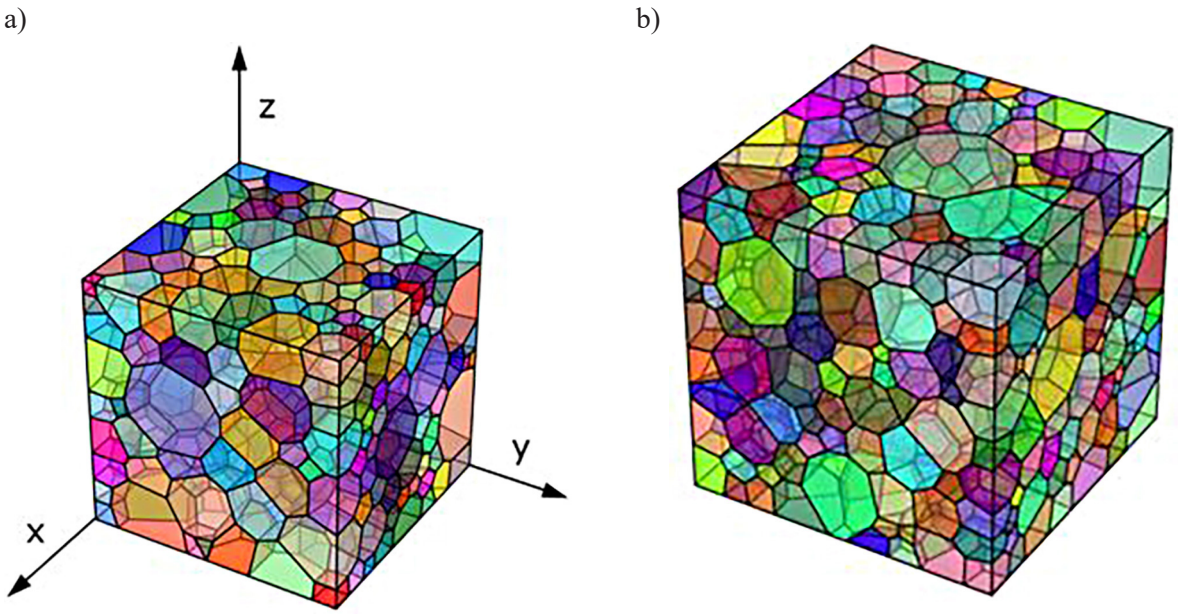

Fig. 8. RVE divided into 400 (a) and 800 (b) grains

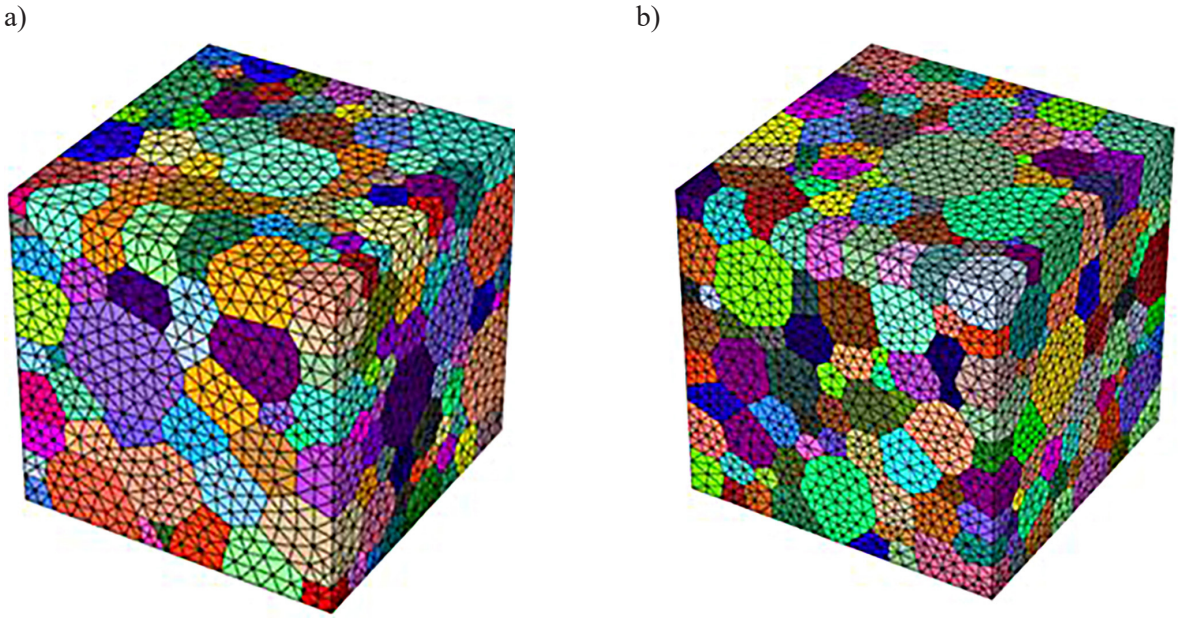

Fig. 9. FEM meshes for RVE with 400 (a) and 800 (b) grains

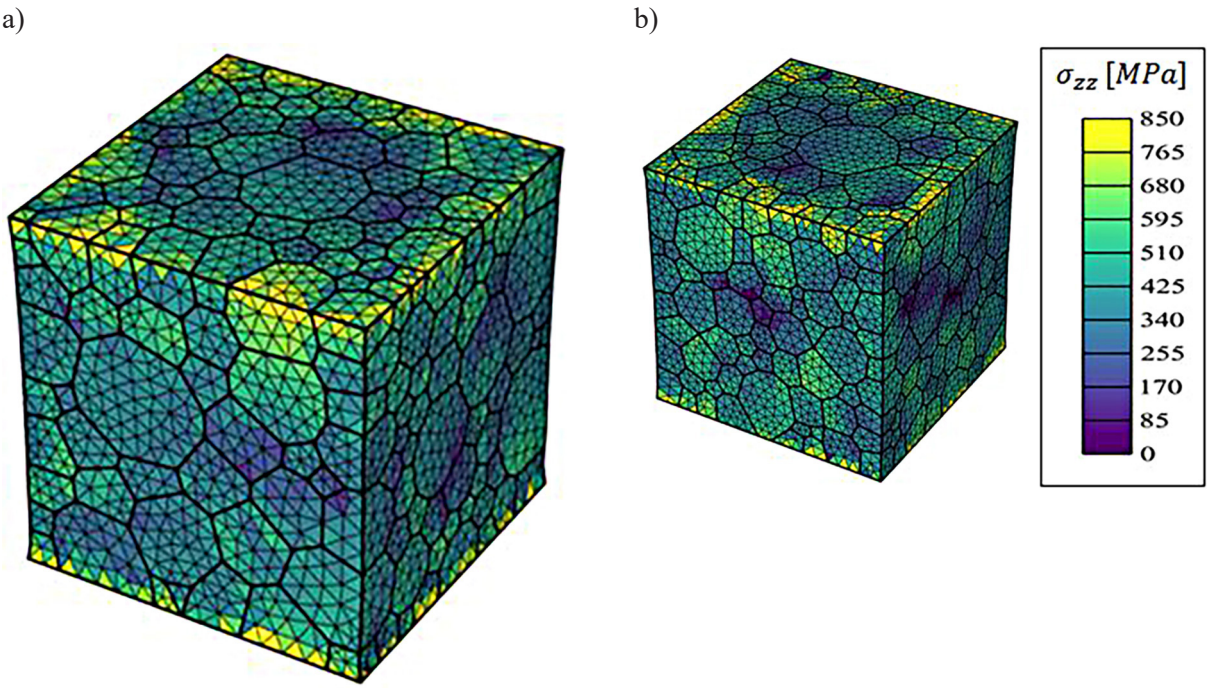

Fig. 10. Distribution of σ_{zz} stress in 400 (a) and 800 (b) grains samples

can be observed. In the middle part of the material the majority of the stresses are in the range 340–425 MPa.

As the result of homogenization, the macroscopic stress-strain curve was computed. The homogenized stress is found as the sum of vertical reactions divided by the actual cross section (computed with the assumption of the volume conservation). The macroscopic stress-strain relationship is shown in Figure 11.

The distribution of equivalent plastic strain for samples with a different number of grains is presented in Figure 12. The strain is mostly in the range 0.018–0.02 and the strong influence of applied boundary conditions is clearly seen. Inhomogeneous distribution of the equivalent plastic strain was noted. Some of grains show higher plastic strains than others, which is associated with the anisotropy of the material.

As another benchmark test, 400 and 800 grains samples (the same as in the previous task) are subjected to shear which was modelled as a compression in *x* direction with the stress value of –180 MPa and as a tension in *z* direction with +180 MPa stress value (the coordinate system is the same as in the tension test). This way pure shear state is obtained in the specimen. Boundary conditions of *triaxial* type in FEPX are applied. In this type of BCs, normal velocities on x = 0, y = 0, z = 0 faces are zeros (the triple symmetry is assumed). In this example material data are the same as in the previous tension test.

The distribution of von Mises stress (H-M-H stress) for both samples with different number of grains is shown in Figure 13. Usually effective stresses are in the range 280–315 MPa. The stress distribution is more regular than in the previous

Table 3. FEM models data – the cubic RVE

Feature	Number of grains	
	400	800
Number of nodes	67 966	132 650
Number of elements	75 802	149 759

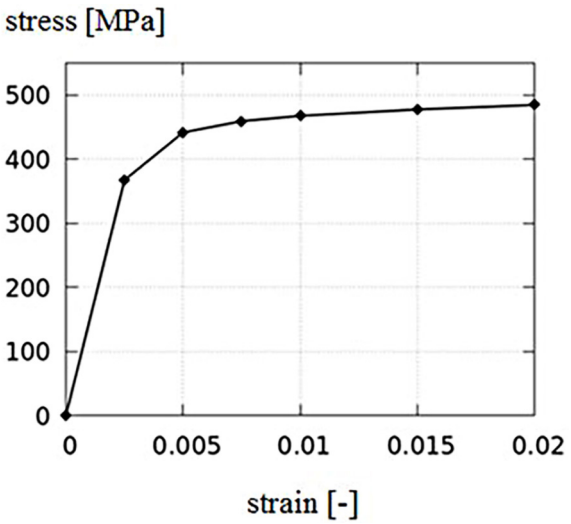

Fig. 11. Macroscopic stress-strain curve

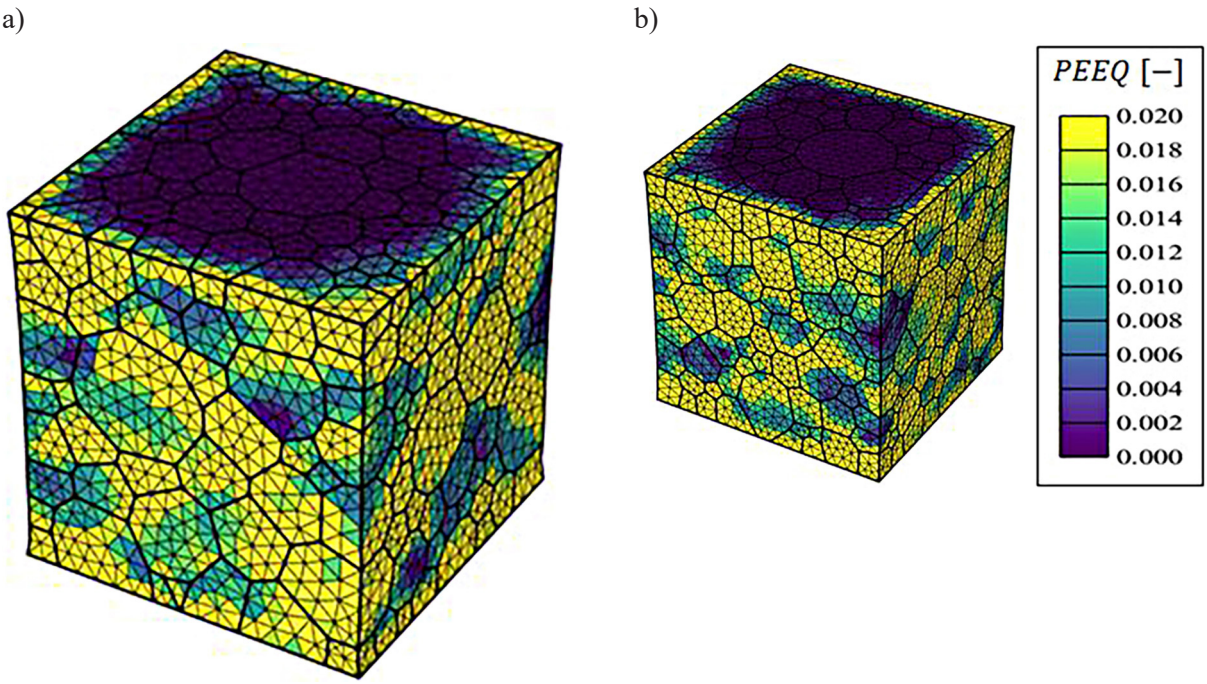

Fig. 12. Distribution of equivalent plastic strain (PEEQ) for 400 (a) and 800 (b) grains samples

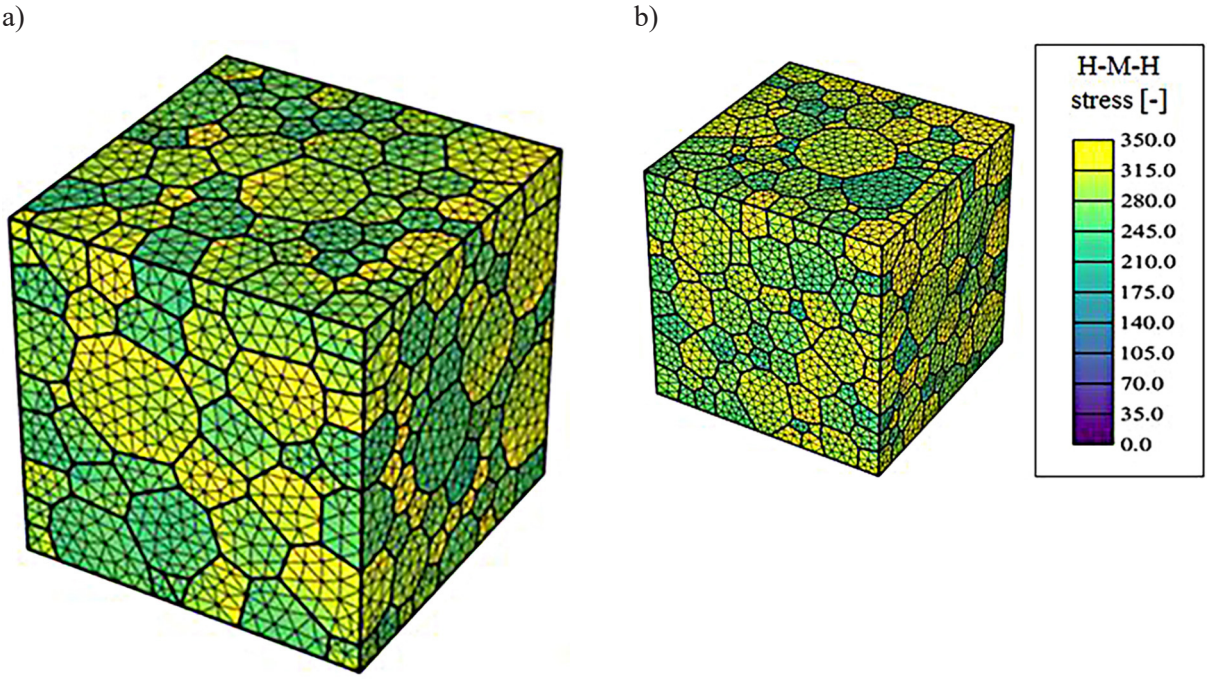

Fig. 13. Distribution of H-M-H stress for 400 (a) and 800 (b) grains samples

tension test. The influence on boundary conditions is negligible.

In further benchmark test a paddy-like shape sample of overall dimensions 1.0 × 0.2 × 4.0 mm was subjected to tension load. Once again, in the tessellation process 400 and 800 grains were generated. Finite element meshes for both samples are shown in Figure 14. The detailed data of FEM models is contained in Table 4. The global coordinate system, boundary conditions and material data are the same as in the tension benchmark test.

The stress and equivalent plastic strain distributions are presented in Figures 15 and 16. In both 400 and 800 grain models, strain localization next to the notch is visible. The results obtained for denser mesh are more reliable. It is very interesting that for both samples shearing bands can be clearly observed (contours sloped at 45 angle).

a) b)

Fig. 14. Meshes for 400 (a) and 800 (b) grains samples

Table 4. FEM models data – paddy-like shape sample

Feature	Number of grains	
	400	800
Number of nodes	73 899	140 284
Number of elements	79 851	153 448

CONCLUSIONS

In this paper numerical simulations of an uniaxial loading and a shear test were done using the crystal plasticity finite element method (CPFEM). The change of the microstructure and dislocation slip as the mechanism of the plastic deformation are considered here. Benchmark tests presented here were performed for the C11000 copper alloy of FCC crystalline structure. Numerical calculations were done for a different number of grains assuming its random distribution and orientation. Three benchmark tests are made: the tension and shearing test of the cube sample and the tension test of paddy-like sample. Stress and equivalent plastic strain distributions are presented. Additionally, macroscopic response as the stress-strain curve was also generated as the result of homogenization. The results obtained show the inhomogeneity of stress and strain in samples associated with the anisotropy of grains.

The main conclusions resulting from included benchmark tests are summarized as follows. The CPFEM software enables to solve elastic-plastic problems taking into consideration the mechanism of the plastic deformation – in this paper a dislocation slip. The inhomogeneous behaviour of the material under loading (tension or shear) was noted. It is caused by the anisotropy of material resulting from different crystals orientation. The application of a crystal plasticity theory in solving elastic-viscoplastic problems gives a more realistic description of material behaviour under loading. However, this is a time-consuming process which in practice should be

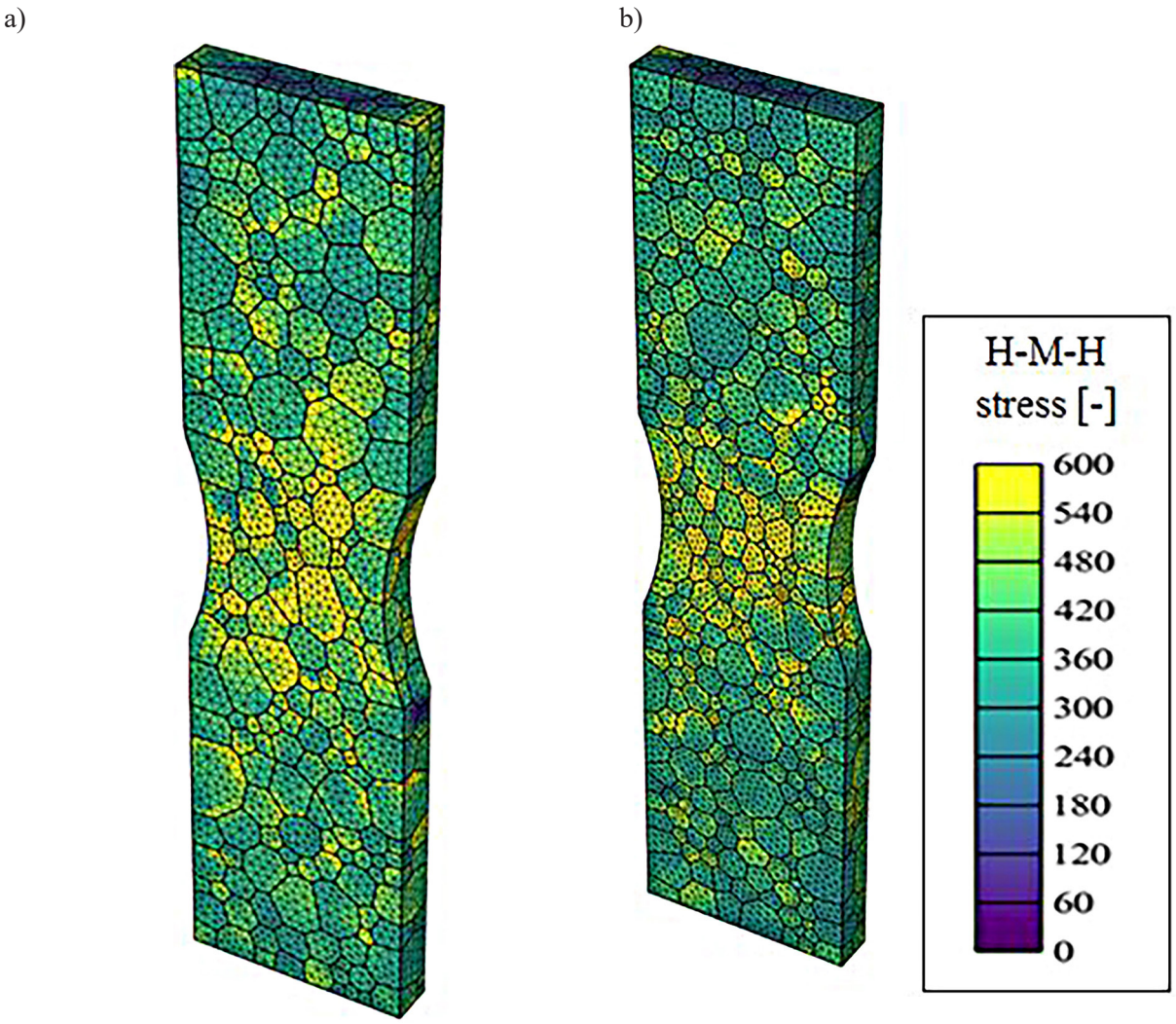

Fig. 15. Distribution of H-M-H stress for 400 (a) and 800 (b) grains samples

executed on powerful workstations. Experimental validation of crystal plasticity models may not be limited to verify the results obtained in macro scale only (e.g. homogenization of stress-strain curve). It should also contain comparisons of experimental and numerical data in the nano-scale. The change of crystals orientations after deformation plotted in the form of pole figures is a good example. Unfortunately, the electron back scatter diffraction (EBSD) equipment is not available for the authors. For this reason experimental verification of numerical results in nano-scale is out of scope of this paper.

In this paper the potential of crystal plasticity theory in solving elastic-plastic problems has been presented on relatively simple benchmark tests. Computations have been executed on PC computer and they have taken from one hour (400 grains cube subjected to tension) to twelve hours (paddy-like sample with 800 grains). However, it is worth noting that the results are valuable. It is very important that even simple models can predict a properly materials elastic-plastic response. Here, for instance, even 400 grains paddy-like sample presents shearing bands.

Open source software for crystal plasticity finite element method available on the internet is usually restricted to make analyses of simple shape models (cube, cylinder) for which simple boundary conditions and simple loads can be applied. It is not possible to apply, e.g. contact conditions typical in simulations of material processing. In the future research authors intend to develop crystal plasticity user material procedures which will be linked with the commercial FEM software. This way more sophisticated elastic-plastic problems (rolling, extrusion etc.) may be solved. The results of benchmark tests presented in this paper will be used as reference solutions in the validation of developed user material programs.

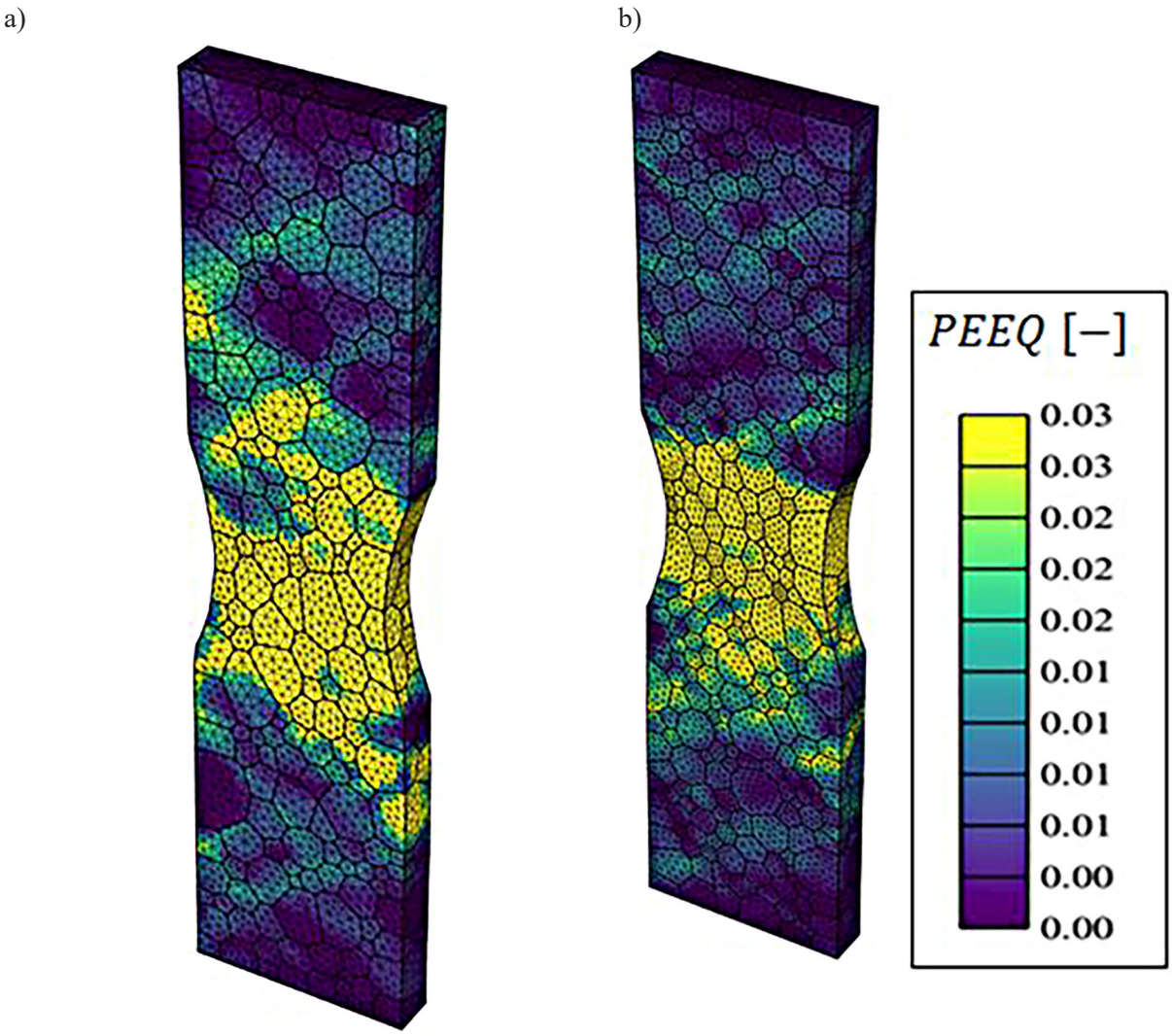

Fig. 16. Distribution of PEEQ for 400 (a) and 800 (b) grains samples

REFERENCES

1. Szala M., Winiarski G., Bulzak T.A., Wójcik Ł. Microstructure and Hardness of Cold Forged 42CrMo4 Steel Hollow Component with the Outer Flange. Advances in Science and Technology Research Journal. 2022; 16(4): 201–210. https://doi.org/10.12913/22998624/152790
2. Wojtacha A., Opiela M. Effect of Plastic Deformation on CCT-Diagram of Multi-Phase Forging Steel. Advances in Science and Technology Research Journal. 2021; 15(4): 72–80. https://doi.org/10.12913/22998624/142473
3. Chocyk D., Zientarski T. Effect of Nanoindentation Rate on Plastic Deformation in Cu Thin Films. Advances in Science and Technology Research Journal. 2022; 16(1): 170–179. https://doi.org/10.12913/22998624/142775
4. Yang G., Park S.-J. Deformation of Single Crystals, Polycrystalline Materials, and Thin Films: A Review. Materials. 2019; 12: 2003. https://doi.org/10.3390/ma12122003.
5. Subrahmanyam Pattamatta A.S.L., Srolovitz D.J. Allotropy in ultrahigh strength materials. Nature Communications. 2022; 13: 3326. https://doi.org/10.1038/s41467-022-30845-z
6. Zecevic M., Lebensohn R.A., McCabe R.J., Knezevic M. Modeling of intragranular misorientation and grain fragmentation in polycrystalline materials using the viscoplastic self-consistent formulation. International Journal of Plasticity. 2018; 109: 193–211. https://doi.org/10.1016/j.ijplas.2018.06.004
7. Khan R., Pervez T., Alfozan A., Qamar S.Z., Mohsin S. Numerical Modeling and Simulations of Twinning-Induced Plasticity Using Crystal Plasticity Finite Element Method. Crystals. 2022; 12, 930. https://doi.org/10.3390/cryst12070930.
8. Kazim S.M., Prasad K., Chakraborty P. A Novel Homogenized Crystal Plasticity Model for Near α and α + β Titanium Alloys. Transitions of the Indian National Academy of Engineering. 2022; 7: 441–

447. https://doi.org/10.1007/s41403-021-00297-w

9. Roters F., Eisenlohr P., Hantcherli L., Tjahjanto D.D., Bieler T.R., Raabe T. Overview of constitutive laws, kinematics, homogenization and multiscale methods in crystal plasticity finite-element modeling: Theory, experiments, applications. Acta Materialia. 2010; 58(4): 1152–1211. https://doi.org/10.1016/j.actamat.2009.10.058
10. Ryś M., Forest S., Petryk H. A micromorphic crystal plasticity model with the gradient-enhanced incremental hardening law. International Journal of Plasticity. 2020; 128: 102655. https://doi.org/10.1016/j.ijplas.2019.102655
11. Kowalczyk-Gajewska K., Mróz Z., Pęcherski R.B. Micromechanical modelling of polycrystalline materials under non-proportional deformation paths. Archives of Metallurgy and Materials. 2007; 52(2): 181–192.
12. Kowalczyk-Gajewska K., Szwiertnia K., Kawałko J., Wierzbanowski K., Wronski M., Frydrych K., Stupkiewicz S., Petryk H. Texture evolution in titanium on complex deformation paths: Experiment and modeling. Materials Science and Engineering: A. 2015; 637: 251–263. https://doi.org/10.1016/j.msea.2015.04.040
13. Petryk H. A quasi-extremal energy principle for non-potential problems in rate-independent plasticity. Journal of Mechanics and Physics of Solids. 2020; 136: 103691. https://doi.org/10.1016/j.jmps.2019.103691
14. Frydrych K. Simulations of grain refinement in various steels using the three-scale crystal plasticity model. Metallurgical and Materials Transactions A. 2019; 50(10): 4913–4919. https://doi.org/10.1007/s11661-019-05373-z
15. Frydrych K., Kowalczyk-Gajewska K. A three-scale crystal plasticity model accounting for grain refinement in FCC metals subjected to severe plastic deformations. Materials Science and Engineering: A 2016; 658: 490–502. https://doi.org/10.1016/j.msea.2016.01.101
16. Roters F., Eisenlohr P., Bieler T.R. and Raabe D. Crystal Plasticity Finite Element Methods: In Materials Science and Engineering. Wiley, 2010.
17. Riddle S.K., Wilson T.R., Rajivmoorthy M., Eberhart M.E. Principles Determining the Structure of Transition Metals. Molecules. 2021; 26: 5396. https://doi.org/10.3390/molecules26175396
18. Lehtinen A., Laurson L., Granberg F., Nordlund K., Alva M.J. Effects of precipitates and dislocation loops on the yield stress of irradiated iron. Scientific Reports. 2018; 8: 6914. https://doi.org/10.1038/s41598-018-25285-z
19. Girard G., Frydrych K., Kowalczyk-Gajewska K., Martiny M., Mercier S. Cyclic response of electrodeposited copper films. Experiments and elastic–viscoplastic mean-field modeling. Mechanics of Materials. 2021; 153: 103685. https://doi.org/10.1016/j.mechmat.2020.103685
20. Kursa M. Modeling of plastic deformation in metal crystals by incremental energy minimization. Institute of Fundamental Technological Research Polish Academy of Sciences, 2010.
21. Dakshinamurthy M., Kowalczyk-Gajewska K., Vadillo G. Influence of crystallographic orientation on the void growth at the grain boundaries in bicrystals. International Journal of Solids and Structures. 2021; 212: 61–79. https://doi.org/10.1016/j.ijsolstr.2020.11.035
22. Petryk H., Stupkiewicz S., Kucharski S. On direct estimation of hardening exponent in crystal plasticity from the spherical indentation test. International Journal of Solids and Structures. 2017; 112: 209–221. https://doi.org/10.1016/j.ijsolstr.2016.09.025
23. Mánik T., Asadkandi H.M., Holmedal M. A robust algorithm for rate-independent crystal plasticity. Computer Methods in Applied Mechanics and Engineering. 2022; 393: 114831. https://doi.org/10.1016/j.cma.2022.114831
24. Frydrych K. Modeling of the evolution of the microstructure of metals with high specific strength in the processes of intensive plastic deformation. Institute of Fundamental Technological Research Polish Academy of Sciences, 2017.
25. Frydrych K., Jarzębska A., Virupakshi S., Kowalczyk-Gajewska K., Bieda M., Chulist R., Skorpuska M., Schell N., Sztwiernia K. Texture-based optimization of crystal plasticity parameters: application to zinc and its alloy. Metallurgical and Materials Transactions A – Physical Metallurgy and Materials Science. 2021; 52(8): 3257–3273. https://doi.org/10.1007/s11661-021-06285-7
26. Frydrych K., Libura T., Kowalewski Z., Maj M., Kowalczyk-Gajewska K. On the role of slip, twinning and detwinning in magnesium alloy AZ31B sheet. Materials Science and Engineering A – Structural Materials Properties Microstructure and Processing. 2021; 813: 141152. https://doi.org/10.1016/j.msea.2021.141152
27. Frydrych K., Maj M., Urbański L., Kowalczyk-Gajewska K. Twinning-induced anisotropy of mechanical response of AZ31B extruded rods. Materials Science & Engineering A. 2020; 771: 138610. https://doi.org/10.1016/j.msea.2019.138610
28. Kowalczyk-Gajewska K., Stupkiewicz S., Frydrych K., Petryk H. Modelling of Texture Evolution and Grain Refinement on Complex SPD Paths. IOP Conference Series: Materials Science and Engineering. 2014; 63: 012040. http://iopscience.iop.org/1757-899X/63/1/012040
29. Rezaee-Hajidehi M., Sadowski P., Stupkiewicz S. Deformation twinning as a displacive transforma-

tion: Finite-strain phase-field model of coupled twinning and crystal plasticity. Journal of the Mechanics and Physics of Solids. 2022; 163: 104855. https://doi.org/10.1016/j.jmps.2022.104855

30. Nguyen K., Zhang M., Amores V.J., Sanz M.A., Montáns F.J. Computational Modeling of Dislocation Slip Mechanisms in Crystal Plasticity: A Short Review. Crystals. 2021; 11: 42. https://doi.org/10.3390/cryst11010042
31. Kowalczyk-Gajewska K. Modelling of texture evolution in metals accounting for lattice reorientation due to twinning. European Journal of Mechanics – A/Solids. 2010; 29(1): 28–41. https://doi.org/10.1016/j.euromechsol.2009.07.002
32. Yaghoobi M., Ganesan S., Sundar S., Lakshmanan A., Rudraraju S., Allison J.E., Sundararaghavan V. PRISMS – Plasticity: An open-source crystal plasticity finite element software. Computational Materials Science. 2019; 169: 109078. https://doi.org/10.1016/j.commatsci.2019.109078
33. Kucharski S., Stupkiewicz S., Petryk H. Surface Pile-Up Patterns in Identation Testing of Cu Single Crystals. Experimental Mechanics. 2014; 54: 957–969. https://doi.org/10.1007/s11340-014-9883-1
34. Lu D., Zhang K., Hu G., Lan Y., Chang Y. Investigation of Yield Surfaces Evolution for Polycrystalline Aluminum after Pre-Cyclic Loading by Experiment and Crystal Plasticity Simulation. Materials. 2020; 13: 3069. https://doi.org/10.3390/ma13143069
35. Nguyen N., Wass A.M. Nonlinear, finite deformation, finite element analysis. Journal of Applied Mathematics and Physics. 2016; 67: 35. https://doi.org/10.1007/s00033-016-0623-5
36. Han X., Besson J., Forest S., Tanguy B., Bugat S. A yield function for single crystals containing voids. International Journal of Solids and Structures. 2013; 50(14–15): 2115–2131. https://doi.org/10.1016/j.ijsolstr.2013.02.005
37. Kowalczyk K., Gambin W. Model of plastic anisotropy evolution with texture-dependent yield surface. International Journal of Plasticity. 2004; 20: 19–54. https://doi.org/10.1016/S0749-6419(03)00010-X
38. Dawson P.R., Boyce D.E., Park J.S., Wielewski E., Miller M.P. Determining the strengths of HCP slip systems using harmonic analyses of lattice strain distributions. Acta Materialia. 2018; 144: 92–106. https://doi.org/10.1016/j.actamat.2017.10.032
39. Zhang K.S., Shi Y.K., Ju J.W. Grain-level statistical plasticity analysis on strain cycle fatigue of a FCC metal. Mechanics of Materials. 2013; 64: 76–90. https://doi.org/10.1016/j.mechmat.2013.05.001
40. Engel B., Huth M., Hyde C. Numerical Investigation into the Influence of Grain Orientation Distribution on the Local and Global Elastic-Plastic Behaviour of Polycrystalline Nickel-Based Superalloy INC-738 LC. Crystals. 2022; 12: 100. https://doi.org/10.3390/cryst12010100
41. Turkmen H.S., Miller M.P., Dawson P.R., Moosbrugger J.C. A Slip-Based Model for Strength Evolution During Cyclic Loading. Journal of Engineering Materials and Technology. 2004; 126: 329–338. https://doi.org/10.1115/1.1789967